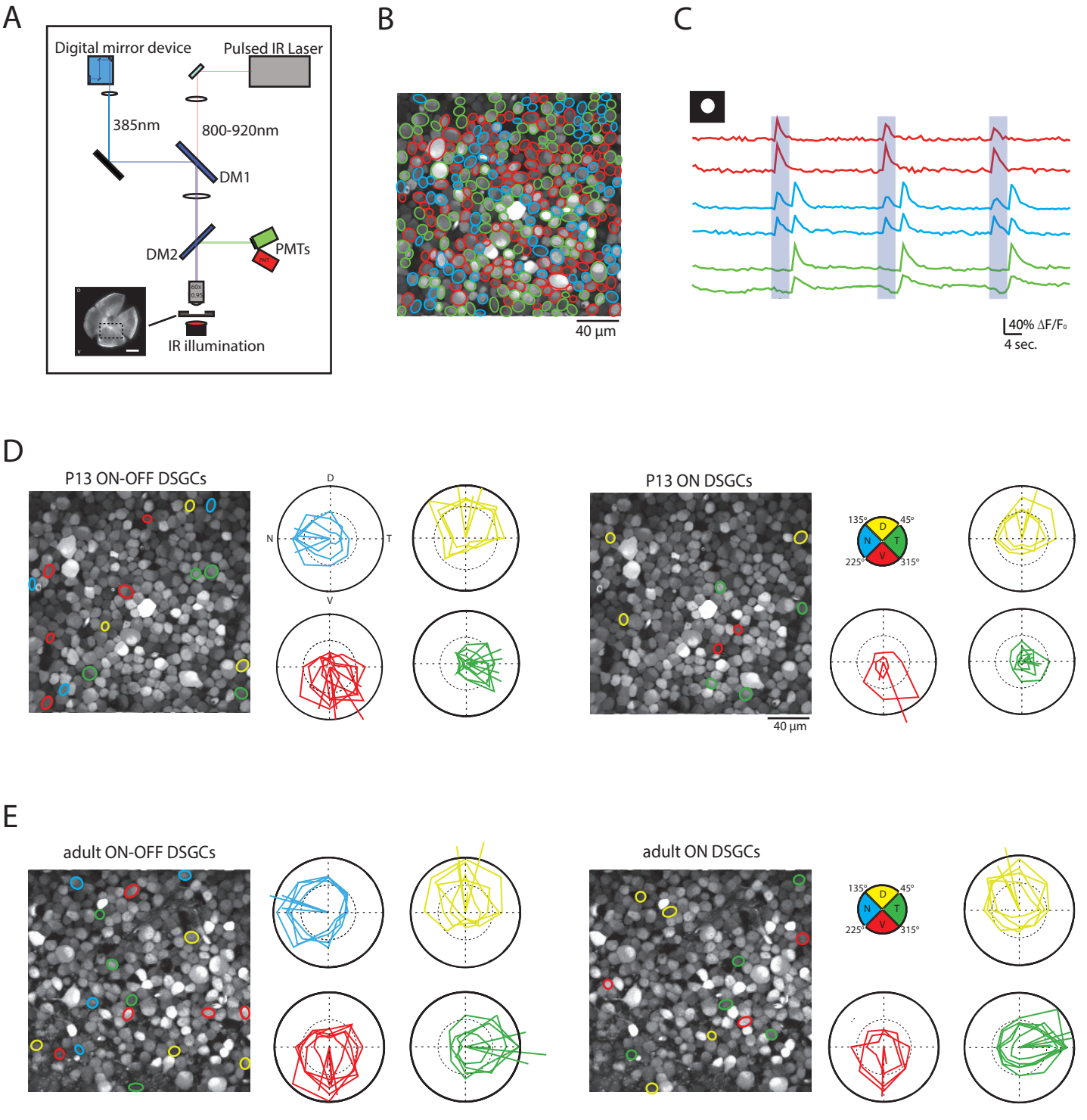
A
Digital mirror device
Pulsed IR Laser
385nm
800-920nm
DM1
DM2
PMTs
IR illumination
B
40 µm
C
40% ΔF/F₀
4 sec.
D
P13 ON-OFF DSGCs
D
N
T
V
P13 ON DSGCs
135°
45°
225°
315°
40 µm
E
adult ON-OFF DSGCs
adult ON DSGCs

Figure S2 related to Figure 2

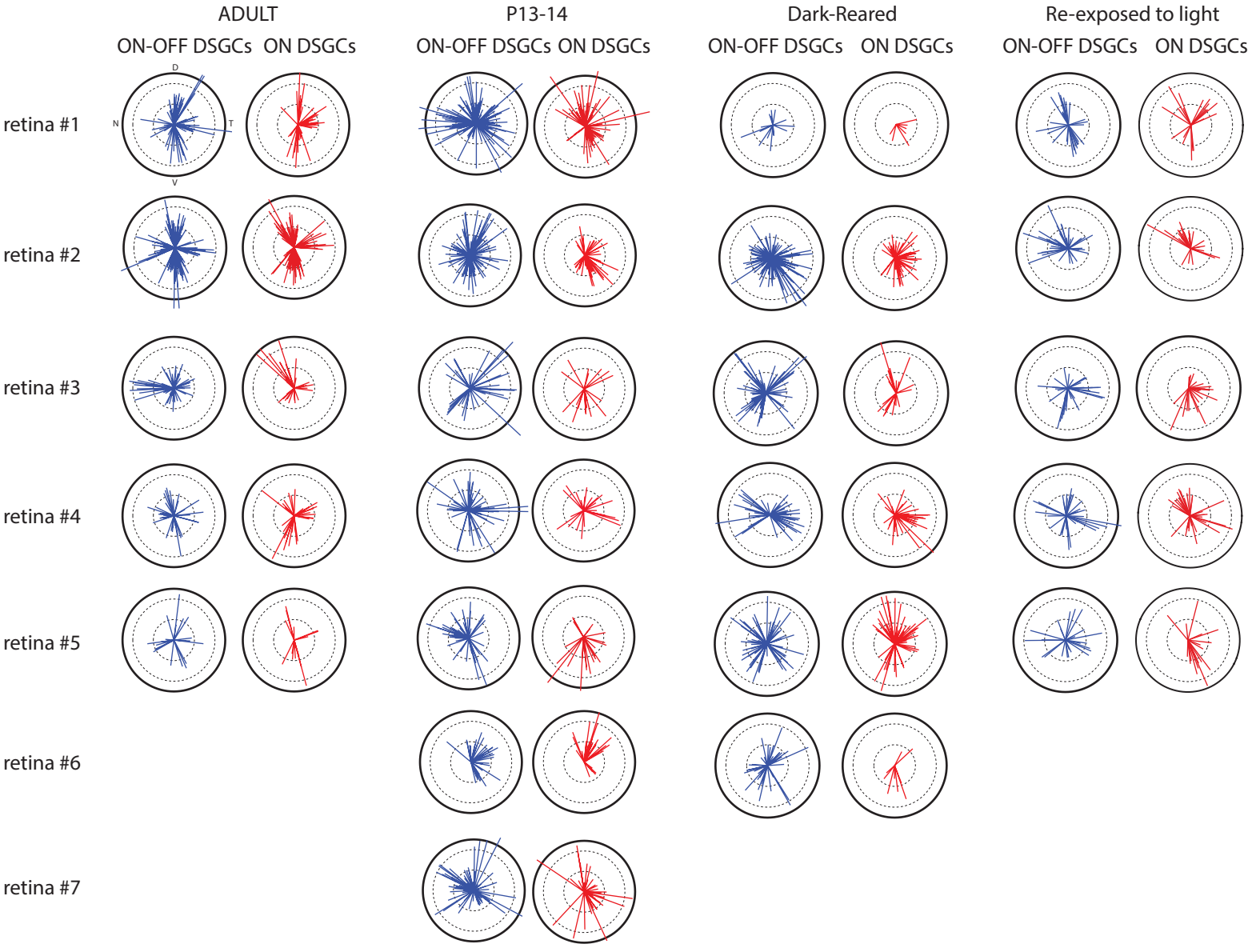

Figure S3 related to Figure 2

ON-OFF

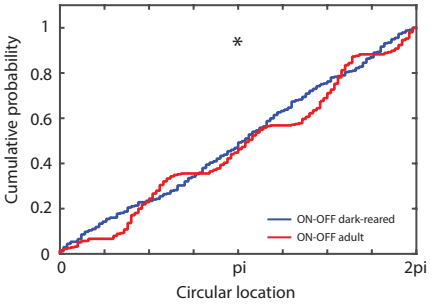

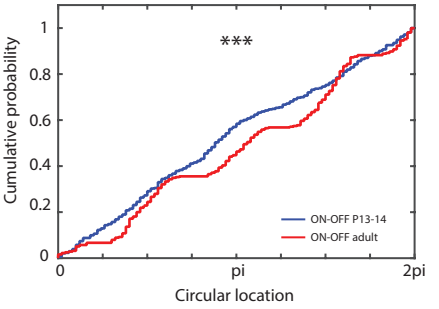

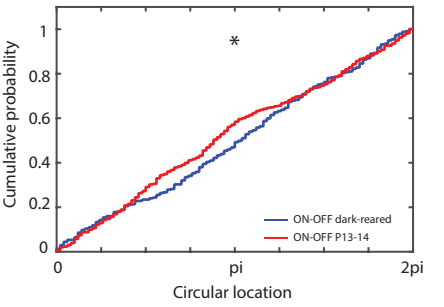

ON-OFF

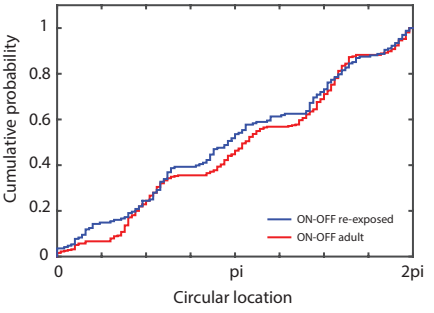

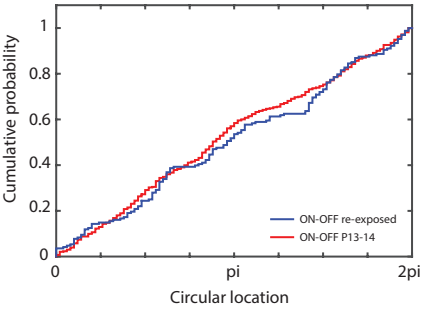

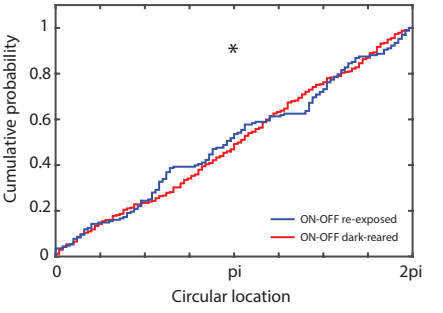

ON

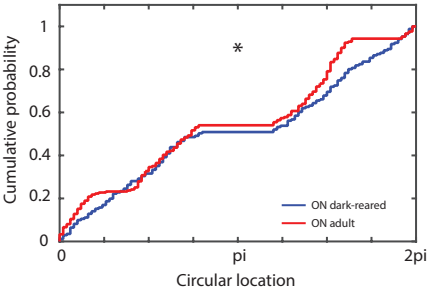

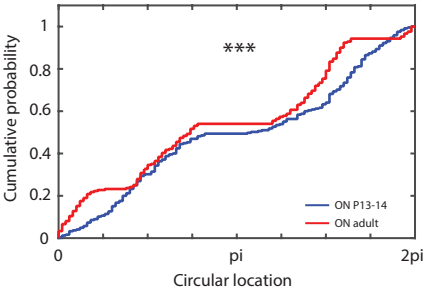

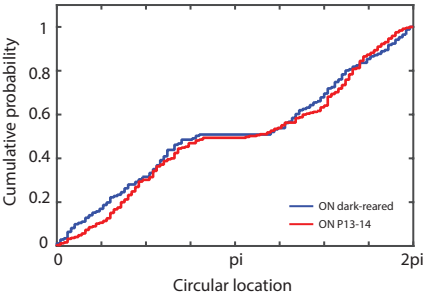

ON

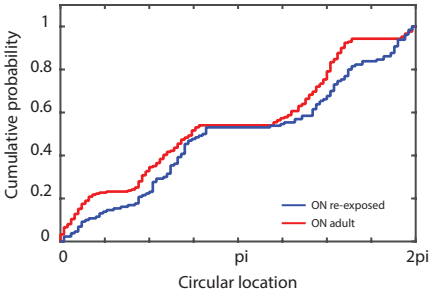

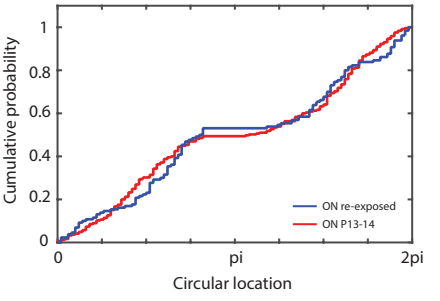

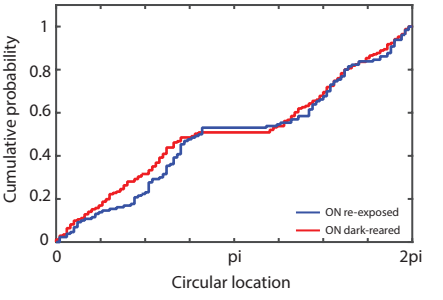

a

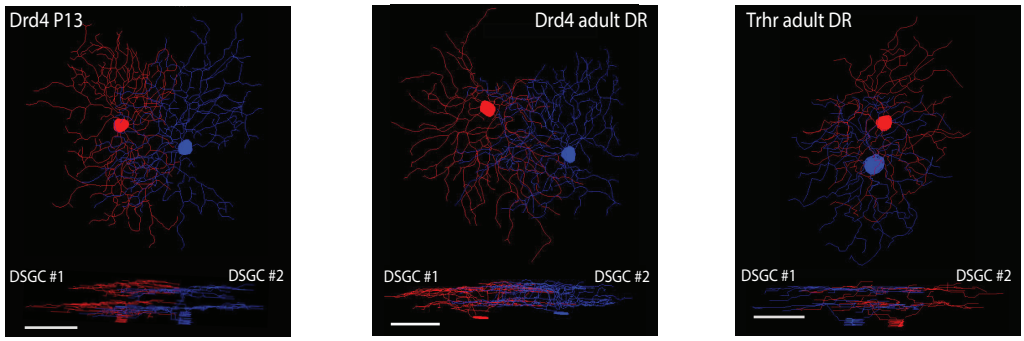
Drd4 P13
DSGC #1
DSGC #2
Drd4 adult DR
DSGC #1
DSGC #2
Trhr adult DR
DSGC #1
DSGC #2

b

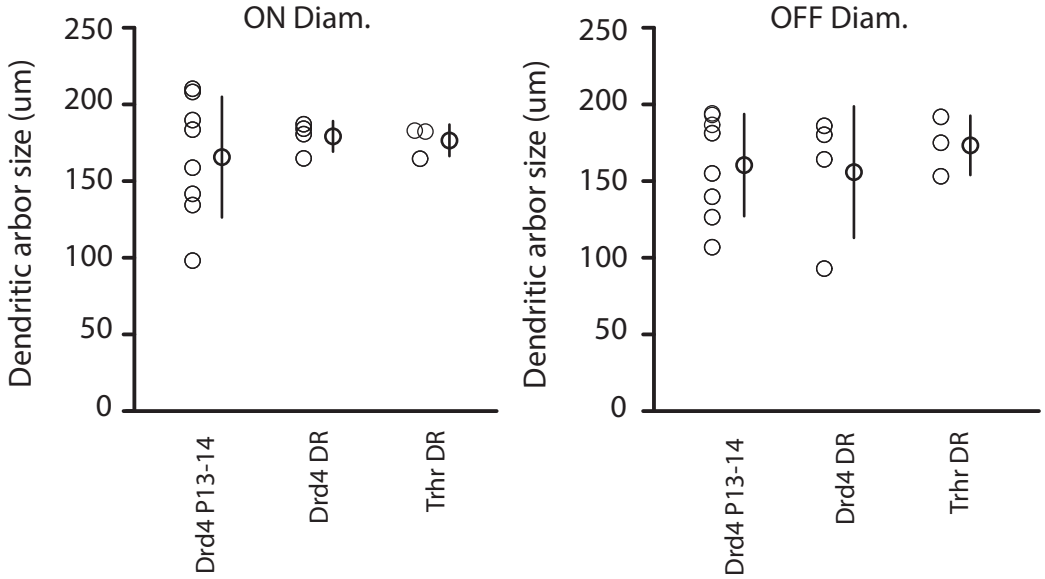
ON Diam.
Dendritic arbor size (um)
250
200
150
100
50
0
Drd4 P13-14
Drd4 DR
Trhr DR
OFF Diam.
Dendritic arbor size (um)
250
200
150
100
50
0
Drd4 P13-14
Drd4 DR
Trhr DR

Legends Supplemental Figures

Figure S1 related to Figure 1: Customized microscope for two-photon calcium imaging of UV-light responses of distinct DSGCs in acutely isolated retina.
(A) Schematic of the modified two-photon microscope (see Suppl. Experimental Procedures for a detailed description). PMTs, photo multiplier tubes. DM, dichroic mirror. *Insert:* Isolated retina mounted ganglion cell side up on a ring-supported hydrophilized PTFE membrane. Dotted line marks imaging region. D, dorsal and V, ventral. Scale bar, 1 mm
(B) Two-photon fluorescent image of OGB-1 in ganglion cell layer of P13 retina. Red, blue and green circles indicate ON, ON-OFF and OFF RGCs, respectively.
(C) Examples of fractional change in OGB-1 fluorescence ($\Delta F/F_o$) averaged over the somas of six RGCs in the same field of view in response to three consecutive full-field UV flashed spots (blue areas). ON, red traces; ON-OFF, blue traces; OFF, green traces, P13 retina
(D) *Left:* Two-photon fluorescent image of OGB-1 in ganglion cell layer of P13 retina with somas of different DSGC subtypes (blue, yellow, red and green circles indicate nasal, dorsal, ventral and temporal subtypes, respectively) for the ON-OFF DSGCs and the ON DSGCs. *Right:* Tuning curves derived from $\Delta F/F_o$ of circled DSGC subtypes. External solid black lines from polar plots are indicating the amplitude of calcium signals (normalized to maximal $\Delta F/F_o$)
(E) Same as D for P36 retina.

Figure S2 related to Figure 2: The diffuse distribution of the preferred directions of DSGCs along the cardinal axes at P13-14 and after dark-rearing was present in each individual preparation. Re-exposure of dark-reared mice to light partially reversed this effect. Polar plots of the preferred directions of ON-OFF DSGCs (blue) and ON DSGCs (red) in adult (left), at P13-14 (middle left), after dark-rearing (middle right) and after re-exposure of dark-reared mice to light for 30-50 days (right). Each row corresponds to one retina in each condition.

Figure S3 related to Figure 2. Effect of visual experience on the distribution of preferred directions of DSGCs. Comparisons of cumulative distribution functions of the preferred directions of the ON-OFF DSGCs (top) and the ON DSGCs (bottom) in the four different conditions (adult, eye-opening, dark-rearing, re-exposed to the light after dark-rearing) (*, $p<0.05$; ***, $p<0.001$, Kuiper's test). See also Table S3.

Figure S4 related to Figure 4. Dark-rearing did not induce changes of the dendritic bi-stratification of ON-OFF DSGCs. (A) *Top*, Neurolucida reconstructions of two neighboring DRD4 GFP+ DSGCs at P13 (*left*), two neighboring dark-reared DRD4 GFP+ DSGCs (*middle*) and two neighboring dark-reared TRHR GFP+ DSGCs (*right*). All the cells were sequentially filled with fluorescent molecule Alexa 594 and Alexa 488 via a patch pipette as described in [S1]. *Bottom*, XZ sections of reconstructed cells. Scale bar, 50 μm. DSGC, direction selective ganglion cell; DR, dark-reared; P13, post-natal day 13. **(B)** *Left*, Average diameter of the dendritic arbor in the ON (*left*) and the OFF (*right*) sub-laminae of the inner plexiform layer (IPL) from P13 DRD4-GFP cells (left, n=5 cells from 2 retinas), dark-reared DRD4-GFP cells (middle, n=5 cells from 2 retinas) and dark-reared TRHR-GFP cells (right, n=3 cells from one retina) (ns, one-way ANOVA with Tukey post-hoc test).

			All RGCs	All RGCs	All RGCs	All RGCs	DSGCs	DSGCs
	No. of Retinas	No. of Cells	% ON	% OFF	% ON-OFF	% NR	% ON	% ON-OFF
P13-14	7	4473	41.87	30.10	28.03	19.15	5.50	9.68
Adult (>P30)	5	2647	44.44	34.71	20.84	18.80	8.10	11.9
Dark-reared	6	3972	38.74	32.02	29.24	27.91	4.31	8.51
Re-exposed to light	5	3107	45.22	38.02	16.76	27.66	4.24	7.47

Table S1 related to Figure 1-2. Effect of visual experience on the percentage of RGC and DSGC types (DSI>0.3) detected with two-photon calcium imaging in response to UV stimulation; RGCs, retinal ganglion cells, DSGCs, direction-selective ganglion cells; NR, non responsive cells; DSI, direction selectivity index; P13-14 and P30, post-natal days 13-14 and 30, respectively (*, $p<0.05$; **, $p<0.01$; ***, $p<0.001$, one-way ANOVA with Tukey post-hoc test).

ON-OFF DSGCs	**p1 (0°)**	**p2 (90°)**	**p3 (180°)**	**p4 (270°)**	**κ1 (0°)**	**κ2 (90°)**	**κ3 (180°)**	**κ4 (270°)**
Adult	0.184	0.289	0.212	0.315	13.17	10.78	12.4	11.36
P13-14	0.244	0.405	0.166	0.185	2.061	1.579	6.156	3.446
Dark reared	0.262	0.128	0.381	0.229	1.510	0.000	1.135	0.427
Re-exposed to light	0.288	0.242	0.225	0.245	5.247	9.024	6.496	9.664
ON DSGCs	**p1 (0°)**	**p2 (105°)**	**p3 (263°)**	**κ1 (0°)**	**κ2 (105°)**	**κ3 (263°)**		
Adult	0.285	0.312	0.403	10.21	7.466	7.865		
P13-14	0.486	0.260	0.254	1.202	5.087	3.119		
Dark reared	0.494	0.239	0.267	1.968	7.413	5.251		
Re-exposed to light	0.321	0.389	0.291	4.725	5.337	6.662		

Table S2 related to Figure 2. Parameters of von Mises equation of the preferred directions distributions from ON-OFF (top) and ON (bottom) DSGCs in adult, at eye-opening, in dark-reared and dark-reared mice that are re-exposed to light. p is the weight of each von Mises distribution, κ is the concentration parameter, which is inversely proportional to the width of the distribution around a particular cardinal axis.

$$f(\theta) = \sum_{i=1}^{N} \frac{p_i e^{\kappa \cos(\theta - \mu_i)}}{2\pi I_0(\kappa)}$$

ON-OFF DSGCs	**Adult**	**P13-14**	**Dark reared**	**Re-exposed to light**
Adult	-	$p < 0.001$	$p < 0.02$	$p > 0.1$
P13-14	$p < 0.001$	-	$p < 0.05$	$p > 0.1$
Dark reared	$p < 0.02$	$p < 0.05$	-	$p < 0.05$
Re-exposed to light	$p > 0.1$	$p > 0.1$	$p < 0.05$	-
ON DSGCs	**Adult**	**P13-14**	**Dark reared**	
Adult	-	$p < 0.001$	$p < 0.05$	$p > 0.1$
P13-14	$p < 0.001$	-	$p > 0.1$	$p > 0.1$
Dark reared	$p < 0.05$	$p > 0.1$	-	$p > 0.1$
Re-exposed to light	$p > 0.1$	$p > 0.1$	$p > 0.1$	-

Table S3 related to Figure S3. Kuiper's statistical test of the preferred directions distributions from ON-OFF (top) and ON (bottom) DSGCs in adult, at eye-opening (P13-14), in dark-reared mice, and in dark-reared mice that have been re-exposed to light.

		Drd4	Trhr
Adult (GFP+ cells)	Nasally-tuned	74 % (26/35)	81 % (21/26)
	Temporally-tuned	0 % (0/35)	0 % (0/26)
	Dorsally-tuned	0 % (0/35)	0 % (0/26)
	Ventrally-tuned	0 % (0/35)	0 % (0/26)
	Untuned	26 % (9/35)	19% (5/26)
	Pre-electroporation	164.4 ± 5.7	128.5 ± 7.6
	Post-electroporation	165.0 ± 26.9	110.0 ± 13.1
	Immunostaining	195 §	104.9 §
Eye-opening (GFP+ cells)	Nasally-tuned	46 % (23/50)	46 % (21/46)
	Temporally-tuned	0 % (0/50)	0 % (0/46)
	Dorsally-tuned	8 % (4/50)	6.5 % (3/46)
	Ventrally-tuned	4 % (2/50)	6.5 % (3/46)
	Untuned	42 % (21/50)	41 % (19/46)
	Pre-electroporation	239.7 ± 22.6	165.2 ± 10.7
	Post-electroporation	244.2 ± 26.4	158.5 ± 17.6
	Immunostaining	228.0 ± 21.9	120 §
Dark-rearing (GFP+ cells)	Nasally-tuned	45 % (21/46)	40 % (14/35)
	Temporally-tuned	0 % (0/46)	0 % (0/35)
	Dorsally-tuned	4 % (2/46)	17 % (6/35)
	Ventrally-tuned	17 % (8/46)	14 % (5/35)
	Untuned	33 % (15/46)	29 % (10/35)
	Pre-electroporation	158.7 ± 9.3	149.0 ± 13.0
	Post-electroporation	173.8 ± 19.1	155.0 ± 13.7
	Immunostaining	165.3 ± 23.6	145.3 ± 4.2

Table S4 related to Figure 4. Characterization of GFP+ cells in DRD4 and TRHR mice. For each condition, we determined the percentage of GFP+ cells (DRD4 and TRHR) that were tuned along different cardinal axes (top) and a comparison of the density of GFP+ cells (cells/mm^2) in live tissue before and after electroporation of Rhod2 (bottom). Note these numbers are compared to those determined with immunostaining for GFP we have performed and from a previous study (§ see Rivlin-Etzion et al. 2011). Cells with DSI>0.3 were considered as direction selective. ($p>0.05$, one-way ANOVA with Tukey post-hoc test).

Supplemental Experimental Procedures

Mice. C57BL/6, DRD4-GFP [26], Trhr-GFP [27] mice of both sexes (13 to 86 days old) were used. Animals from different litters were used for each experiment. Sample sizes (number of retinas and/or cells) for each experiment are indicated in figure legends. All animal procedures were completed in strict compliance with a protocol (R308) approved by the University of California (UC) Berkeley Animal Care and Use Comitte and conformed to the NIH Guide for the Care and Use of Laboratory Animals, the Public Health Service Policy, and the SFN Policy on the Use of Animals in Neuroscience Research.

Tissue preparation. The animals were deeply anesthetized with isoflurane inhalation and killed by cervical dislocation or by decapitation. After the eyes were enucleated, the retinas were dissected and the pigment epithelium carefully removed in oxygenated (95% O_2–5% CO_2) Ames's medium (Sigma-Aldrich, St Louis, MO) at room-temperature under infra-red illumination. The orientation of the retinas was based on landmarks in the choroid, as described by [S1]. Under a dissection microscope, an eye cup with the retinal pigment epithelium attached was positioned with both the ganglion cell layer and the dorsal side facing upward. The nasaltemporal axis was aligned with a horizontal stripe running beneath the optic nerve, with a dark-appearing patch in the ventral side. The nasaltemporal side is opposite for left and right eyes. After verifying the orientation, the isolated retinas were then mounted ganglion cell side up on a ring-supported hydrophilized PTFE membrane (Millipore, Billerica, MA; PICM03050) [S2] and transferred in a recording chamber of an upright microscope for imaging. The whole-mount retinas were continuously perfused (3ml/min) with oxygenated Ames's medium at 32-34°C for the duration of the experiment. The remaining retinas were kept dark at room temperature in Ames' medium bubbled with 95% O_2–5% CO_2 until use (maximum 7-8 h).

Electroporation. The green calcium-sensitive dye Oregon Green 488 BAPTA-1, hexapotassium salt cell impermeant (Invitrogen, Grand Island, NY; O-6806) or the red calcium-sensitive dye Rhod-2 tripotassium salt cell impermeant (Invitrogen, Grand Island, NY; R-14220) were electroporated using the ECM-830 Square Wave electroporation System (BTX Harvard apparatus, Holliston, MA) to uniformly label the neurons within the ganglion cell layer. The following parameters were applied : 12V (young retina) or 13V (adult retina) (top electrode, on ganglion cell layer side), 10-ms-pulse-width, 1-Hz-pulse-frequency, 10-squarewave pulses. The ring-supported hydrophilized PTFE membrane was placed between the two caliper electrodes. 8µl of Ames's medium were previously placed on the lower electrode and 5-10µl of OGB-1 (5mM) or Rhod-2 (5mM) was directly put on the tissue. The distance between the two electrodes was fixed at 1.5-2 mm. Immediately after the electroporation, the time to transfer the tissue in the recording chamber was <30sec. All these procedures were performed under dim red illumination.

Two-photon calcium imaging. Two-photon fluorescence measurements were obtained with a modified movable objective microscope (MOM) (Sutter instruments, Novato, CA) and made using an Olympus 60X, 1.00 NA, LUMPlanFLN objective (Olympus America, Melville, NY). Two-photon excitation of OGB-1 or Rhod-2 was evoked with an ultrafast pulsed laser (Chameleon Ultra II; Coherent, Santa Clara, CA) tuned to 800 nm [S3] or 920nm, respectively. The microscope system was controlled by ScanImage software (www.scanimage.org). Scan parameters were [pixels/line × lines/frame (frame rate in Hz)]: [256 × 256 (1.5)], at 2 ms/line. This MOM was equipped with through-the-objective light stimulation and two detection channels for fluorescence imaging.

Visual Stimulation. Visual stimuli were generated using MATLAB software and projected to the photoreceptor layer using a modified video projector (HP AX325AA Notebook Projector Companion; Hewlett-Packard, Houston,TX) displaying a UV light (single LED NC4U134A, peak wavelength 385 nm; Nichia, Torrance, CA). The intensity of the UV stimulus was ~$1.81 * 10^4$ R*/cone/s. To decrease the noise entering the photon multiplier tubes due to UV stimulation, we placed a GG475 Schott glass filter (Chroma Technology, Bellows Falls, VT) in front of the detector path. We used two kinds of stimuli: a series of full-field flashed spots (~200 µm) and a bar (300 × 1000 µm) moving in eight different directions at 0.5 mm/s. Each direction was repeated at least three times. In both cases, the stimulus had a 100% positive contrast (bright on darker background).

Data analysis. Images were analyzed offline using custom MATLAB software. The regions of interest (ROIs) of cells were determined using the Trainable Weka Segmentation (Waikato Environment for Knowledge Analysis) plugin for imageJ, and the pixel intensities within a ROI were averaged at each time step. The fluorescence intensity of a neuron is reported throughout as the average intensity of all pixels over its soma, including the nucleus. The

mean intensity value for each cell was filtered with a rolling ball filter to correct for changing baselines. The rolling ball filter was set to change the baseline fluorescence to match fluorescence during an initial calibration period when UV light stimulation was absent. Fluorescence responses are reported as normalized increases as follows:

$$\Delta F/F=(F-F_0)/F_0$$

where F is instantaneous fluorescence induced by UV light stimulation and F_o is the baseline fluorescence when visual stimulation is absent. Peak amplitudes were determined as the average of the peak $\Delta F/F_o$ over the three repetitions of the same stimulus direction. The preferred direction of the cell was determined by normalizing the peak amplitude in each stimulus direction to the summation of the peak amplitudes in all stimulus directions. The sum of these normalized responses yielded a vector (vector sum) whose direction was the preferred direction of the cell and whose magnitude gave the strength and width of tuning.
The directionally selective index (DSI) was calculated for the two-photon OGB-1 and Rhod-2 signals as:

$$DSI = ([\Delta F/F_0]pref – [\Delta F/F_0]null) / ([\Delta F/F_0]pref + [\Delta F/F_0]null)$$

where, $[\Delta F/F_0]pref$ and $[\Delta F/F_0]null$ are the mean amplitudes of $[\Delta F/F_0]$ evoked by the bars moving in the preferred and null directions, respectively. The null direction was 180 degrees rotated from preferred.

Clustering analysis. K-means clustering analysis in MATLAB software was used to evaluate the pattern of distribution of the preferred directions from both ON and ON-OFF DSGCs (Figure 2). All the lengths of the preferred directions were fixed to 1 and these were transformed into Cartesian coordinates for subsequent angular distance measurement. This method optimizes the set of clusters with respect to the distance between each point and the centroid of its cluster, summed for all points [20]. We compared 2–8 cluster numbers, and we calculated the fitness of clustering by using the silhouette value (SV) [21]:

$$SV(i) = (b(i) – a(i)) / \max(a(i),b(i))$$

where a(i) is the average distance between i and all other data within the same cluster (called measure of cohesion), and b(i) is the average distance between i and all points in the nearest cluster (called measure of separation from the closest other cluster). A SV close to 1 indicates data perfectly clustered, whereas a SV close to 0 reflects data which are ambiguously clustered) [21]. A bin size of 10° was used to plot the histograms of the preferred directions periodicity of DSGCs.

We completed this clustering analysis by fitting each population of DSGC preferred directions to a mixture model composed of multiple von Mises distributions. The probability distribution function was calculated as :

$$f(\theta) = \sum_{i=1}^{N} \frac{p_i e^{\kappa \cos(\theta-\mu_i)}}{2\pi I_0(\kappa)},$$

where

$$\sum_{i=1}^{N} p_i = 1,$$

μ is [0° 90° 180° 270°] for ON-OFF DSGCs and [0° 105° 263°] for ON DSGCs, κ is the concentration parameter, which is inversely proportional to the width of the distribution around a particular cardinal axis, p is the weight of each von Mises distribution, and I_0 is the modified Bessel function of first kind and zero order.
In addition, we used Kuiper's test [S4, S5] (Figure S3; Table S3) to compare distributions of preferred directions to each other.

Non-cardinal DSGCs definition. In adult retina, the preferred directions of the ON and the ON-OFF DSGCs can be separated in 3 and 4 clustered groups, respectively. Each group from ON and ON-OFF DSGCs population was then defined by the angle between the two more distant preferred directions within the same cluster. DSGCs at eye-opening or after dark-rearing, which presented a preferred direction outside of the adult defined groups, were considered as non-cardinal DSGCs.

Intracellular filling and reconstructioin of filled cells. Retinas were mounted ganglion cell layer side up on filter

paper (Millipore, Billerica, MA) and were placed under the microscope in oxygenated (95% O_2–5% CO_2) Ames's medium (Sigma-Aldrich, St Louis, MO) at 32–34°C. GFP+ cells were targeted as described above with a glass microelectrode (3–5MΩ) filled with an internal solution (containing, in mM: 98.3 potassium-gluconate, 1.7 KCl, 0.6 EGTA, 5 $MgCl_2$, 2 Na_2-ATP, 0.3 GTP, and 40 HEPES, pH 7.25, with KOH), as well as fluorescent dye (20 mM Alexa Fluor 594, Invitrogen, Grand Island, NY ; 20 mM Alexa Fluor 488, Invitrogen, Grand Island, NY). We used the whole-cell voltage-clamp configuration for 10-20 min to fill the cell. Next, the dye-filled cells were imaged by the two-photon microscope at 780 nm. Images were acquired at 0.5 μm z-interval using a 60x objective (Olympus LUMPlanFl/IR 60x/ 0.90W). The cells' processes were later reconstructed from image stacks with Neurolucida. In a few of the reconstructed cells we lost individual branches of dendrites due to the limited field of view with the 60x objective (236 μm), which resulted in a small underestimation of the On and Off dendritic arbor diameters.

Retinal histology. Whole-mount retinas were fixed in 4% PFA for 20 min, then washed in block solution [2% donkey serum, 2%bovine serum albumin, 0.3% Triton X-100 in PBS, 3 times, 16 min). Next, retinas were incubated in primary antibodies (1:1000 rabbit anti-GFP, Invitrogen, Grand Island, NY; 1:500 goat anti-ChAT, Millipore, Billerica, MA) for 3 days, and then washed in block solution (3 times, 15 min) and left in block solution at 4°C overnight. The retinas were then incubated in secondary antibody (1:1000 donkey anti-rabbit Alexa Fluor 488, 1:1000 donkey anti-goat Alexa Fluor 568; Invitrogen) at 4°C overnight. Then, they were washed in block solution (5 times, 30 min) and left in PBS overnight. Then, retinas were mounted and coverslipped with Vectashield (Vector Laboratories, Burlingame, CA).

Statistical analysis. Grouped data are presented as mean ± s.d. Data sets were tested for normality, and statistical differences were examined using *t*-test or one-way analysis of variance and Tukey *post hoc* test (Graphpad prism software, La Jolla, CA).

Supplemental References

[S1] Wei, W., Elstrott, J., Feller, M.B. (2010). Two-photon targeted recording of GFP-expressing neurons for light responses and live-cell imaging in the mouse retina. Nat. Protoc. 5, 1347-52.

[S2] Ivanova, E., Toychiev. A.H., Yee, C.W., Sagdullaev, B.T. (2013) Optimized Protocol for Retinal Wholemount Preparation for Imaging and Immunohistochemestry. J. Vis. Exp. (82):e51018

[S3] Firl, A., Sack, G.S., Newman, Z.L., Tani, H., Feller, M.B. (2013) Extrasynaptic glutamate and inhibitory neurotransmission modulate ganglion cell participation during glutamatergic retinal waves. J. Neurophysiol. 106, 1969-78.

[S4] Berens P. (2009) CircStat: A Matlab Toolbox for Circular StatisticsKuiper's test. J. of Statistical Software Volume 31, Issue 10.

[S5] Stephens, M.A. (1965) The goodness-of-fit statistic V*N* : distribution and significance points. Biometrika 52, 309-21.